Title: Loss of circulating CD8α$^+$ NK cells during human *Mycobacterium tuberculosis* infection

Authors: Nezar Mehanna[1,†], Atul Pradhan[1,†], Rimanpreet Kaur[1,†], Theodota Kontopoulos[2], Barbara Rosati[1], David Carlson[1], Nai-Kong Cheung[2], Hong Xu[2], James Bean[2], Katherine Hsu[2], Jean-Benoit Le Luduec[2, ‡], and Charles Kyriakos Vorkas[1,3,4‡]

Affiliations:

[1]Renaissance School of Medicine at Stony Brook University, Stony Brook, NY, 11794

[2]Sloan Kettering Institute, Memorial Sloan Kettering Cancer Center, New York, NY 10065

[3]Department of Microbiology and Immunology, Stony Brook University, Stony Brook, NY 11794

[4]Center for Infectious Diseases, Stony Brook University, Stony Brook, NY, 11794

†, ‡: These authors contributed equally to this manuscript.

*Corresponding author Charles Kyriakos Vorkas, MD, charles.vorkas@stonybrookmedicine.edu, 101 Nicolls Road, Health Sciences Center 15060-I, Stony Brook, NY 11794.

Abstract: Natural Killer (NK) cells can recognize and kill *Mtb*-infected cells in vitro, however their role after natural human exposure has not been well-studied. To identify *Mtb*-responsive NK cell populations, we analyzed the peripheral blood of healthy household contacts of active Tuberculosis (TB) cases and source community donors in an endemic region of Port-au-Prince, Haiti by flow cytometry. We observed higher CD8α expression on NK cells in putative resistors (IGRA- contacts) with a progressive loss of these circulating cells during household-associated latent infection and disease. In vitro assays and CITE-seq analysis of CD8α$^+$ NK cells demonstrated enhanced maturity, cytotoxic gene expression, and response to cytokine stimulation

22 relative to CD8α$^-$ NK cells. CD8α$^+$ NK cells also displayed dynamic surface expression dependent
23 on MHC I in contrast to conventional CD8$^+$ T cells. Together, these results support a specialized
24 role for CD8α$^+$ NK cell populations during *Mtb* infection correlating with disease resistance.

25 **INTRODUCTION**

26 Tuberculosis (TB) remains the leading global cause of death from a single bacterial infection and
27 is a significant public health concern (*1, 2*). Exposure to *Mycobacterium tuberculosis* (*Mtb*) bacilli
28 can result in a broad spectrum of clinical outcomes ranging from clearance of primary infection,
29 asymptomatic latent TB infection (LTBI)—measured by *Mtb* peptide-specific interferon γ release
30 assay (IGRA)—or symptomatic active pulmonary TB disease (*2*). It is estimated that 25% of the
31 global population has evidence of latent infection and 10% will progress to active pulmonary
32 disease (*3*). The host immunologic determinants of these clinical outcomes remain poorly defined
33 and are a major obstacle to designing effective TB vaccines and host-directed therapies to prevent
34 disease. Most TB immunology studies focus on conventional peptide-specific T cells (*4-8*), but
35 the presence of these cells have not been shown to correlate with protection (*9-14*). In contrast,
36 few studies have examined *Mtb*-reactive innate lymphocytes that contribute to *Mtb* clearance (*15-*
37 *18*).

38 Here, we focus on the most abundant innate lymphocytes in mammals: Natural Killer (NK) cells
39 (*19*). NK cells are prevalent in the peripheral blood (0.1-18% of leukocytes) and populate tissue
40 sites such as liver, lung, and mucosal barriers (*20*). They express a broad range of germ-line
41 encoded pattern recognition receptors enabling rapid responses to infection without the need for
42 antigen-specific expansion (*21*). Prior work provides mechanistic evidence for NK cell recognition
43 of intracellular and extracellular *Mtb* in vitro through natural cytotoxicity receptor engagement of

44 *Mtb* cell wall components or stress-induced self-ligands (*22-33*). However, few published studies
45 directly examine NK cell biology during natural *Mtb* transmission in humans (*27, 28, 34*).

46 In this study, we interrogate peripheral blood NK cells in a cohort of household TB contacts in an
47 endemic region in Port-au-Prince, Haiti. We analyzed samples from active TB cases (n=50) and
48 their contacts from the same households (n=50) in addition to interferon-gamma (IFNγ) release
49 assay (IGRA)-matched unrelated donors from the source community without household exposure
50 (n=50). We used spectral flow cytometry to test our hypothesis that specific NK cell
51 subpopulations are activated and expand during household-associated *Mtb* exposure and infection.
52 We identify preserved frequency of CD8α^+ NK cells in blood of uninfected household contacts
53 (IGRA$^-$) with progressive loss of this population during household latent infection and active TB
54 disease. CD8α^+ NK cells demonstrated enhanced responsiveness to cytokine stimulation in vitro
55 compared to CD8α^- NK cells and exhibited dynamic surface expression in culture and after in
56 vitro stimulation. Cellular indexing of transcriptomes and epitopes (CITEseq) revealed largely
57 overlapping transcriptional programs between CD8$\alpha^{+/-}$ NK cells with enhanced expression of
58 select cytotoxicity-associated genes in the CD8α^+ subset. We also observed ubiquitous
59 intracellular NK cell CD8α protein expression. Taken together, our results identify a novel
60 subpopulation of *Mtb*-reactive CD8α^+ NK cells associated with resistance to primary tuberculosis
61 infection.

62 **RESULTS**

63 **Clinical cohort description:**

64 To study early events during the immune response to *Mtb*, we used biobanked samples from a
65 cross-sectional study performed at GHESKIO Centers, Port-au-Prince, Haiti to assemble a clinical

66 cohort of household contacts of active pulmonary TB cases between 2015-2018 (NIH U19
67 AI111143, completed). Out of the total 92 household contacts and 591 community controls
68 enrolled, we randomly sampled an age-, sex-, and IGRA-matched subset of 50 TB household
69 contacts and 50 active TB cases from the same households, as well as 50 source community
70 controls without household exposure, based on peripheral blood mononuclear cell (PBMC)
71 availability and quality control (total N=150). All available specimens from IGRA- contacts were
72 analyzed.

73 Age, sex, IGRA status, and relevant sociodemographic variables are summarized in Table 1. No
74 significant variations were observed in the number of household members, household income,
75 smoking status, or alcohol consumption between groups, consistent with previous work (*15*). Fifty
76 percent of contacts slept in the same room as the active pulmonary TB index case. In the overall
77 study cohort, there were a 50% prevalence of IGRA-positivity in the community controls relative
78 to 75% in contacts, consistent with increased transmission within the household. Among the eleven
79 IGRA- contacts enrolled, only 2 IGRA conversions were detected during 6-month follow-up IGRA
80 testing.

81 **IGRA+ community controls have elevated frequency of mature CD56^{-} NK cells:**

82 We first assessed the frequency of NK cell subpopulations in the clinical cohorts using flow
83 cytometry. Human NK cells were defined by the absence of lineage markers for T cells (CD3),
84 monocytes (CD14), and B cells (CD19), and gated on surface expression of neural cell adhesion
85 molecule (NCAM), CD56, and Fc receptor γRIIIA, CD16 (**Fig. 1A**). We stratified NK cells into
86 three subsets based on expression of CD56: CD56^{-}, CD56^{dim}, and CD56^{bright} (*35, 36*). There was
87 no difference in frequency of total NK cells or CD56^{dim} NK cells between clinical groups (**Fig. 1B**
88 **and 1C center**). IGRA+ community controls had fewer CD56^{bright} NK cells (3.11% vs 5.45%,

89 p=0.006) and more $CD56^-$ NK cells (19.1% vs 12.6%, p=0.002) compared to IGRA- controls or
90 IGRA+ contacts, indicating an accumulation of mature NK cells during latent TB infection within
91 the source community **(Fig. 1C, right and left)**.

92 **IGRA+ contacts demonstrate a loss of circulating $CD16^+$ NK cells:**

93 NK cell activity against *Mtb* depends upon complex combinatory signaling transduced by
94 activating and inhibiting receptors (*37-39*). We next investigated markers of NK cell activation ex
95 vivo. We analyzed representative receptors, including CD16a (FcγRIIIA), which binds the F_c
96 region of antibodies and can induce antibody-dependent cellular cytotoxicity (ADCC). Within the
97 major $CD56^{dim}$ subset, IGRA+ contacts had decreased circulating $CD16^+$ NK cells compared to
98 IGRA+ controls (60% vs 80%, $p < 0.0001$) with a reciprocal increase in $CD16^-$ population,
99 representing downregulation or shedding of CD16 surface expression during household-associated
100 LTBI **(Fig. 2A)** (*40*). We found no significant differences in other canonical markers of NK cell
101 activation ex vivo including activation markers CD69 or CD25, or HLA-E restricted receptor
102 NKG2C. We observed decreased staining for degranulation marker CD107a in $CD56^{bright}$ NK cells
103 of IGRA- contacts, potentially representing recent activation events during household exposure.
104 (**Fig. 2B - D**).

105 **NK cells of IGRA- contacts have a depressed functional phenotype:**

106 To assess functional activity of NK cells in vitro, we cultured PBMCs in media alone or with K562
107 cells—a leukemia cell line with low levels of HLA I expression known to activate NK cells—co-
108 incubated at 1:20 K562:PBMC for 15 hours. Cells were then stained, and percent difference was
109 calculated for CD69, CD107a, CD16, and NKG2C. Our positive control analyses in **Fig. 3A**
110 display results from the major $CD56^{dim}$ subset and demonstrate CD107a, CD69, and NKG2C were

111 significantly increased with K562, while CD16 was significantly decreased, across all clinical
112 groups.

113 Next, we directly compared NK cell response to K562 between clinical groups. IGRA+ contacts
114 demonstrated significantly more degranulation (CD107a) and NKG2C expression after
115 stimulation relative to IGRA- contacts (**Fig. 3B, left)**. IGRA+ contacts also demonstrated
116 depressed CD69 responses relative to IGRA+ controls (**Fig. 3B, top right**). No significant
117 differences in CD16 expression were detected. The same analyses applied to $CD56^{-}$ and $CD56^{bright}$
118 NK cells demonstrated similar responses to stimulation, but no significant differences between
119 clinical groups (**Fig. S1, A - D**). Taken together with our ex vivo data, these in vitro restimulation
120 results indicate that $CD56^{dim}$ NK cells of putative *Mtb* resistors (IGRA- contacts) have depressed
121 function, potentially representing sequelae of recent household-associated *Mtb* exposure.

122 **Loss of circulating $CD8\alpha^{+}$ NK cells during household-associated Mtb infection:**

123 Despite their canonical classification as short-lived innate lymphocytes, NK cells are increasingly
124 recognized for their marked diversity and ability to differentiate into longer-lived effectors (*16,*
125 *18, 27, 41-44*), including after mycobacterial stimuli (*45*). The most extensively studied is an NK
126 cell memory population co-expressing NKG2C and CD57 that expands in blood during human
127 cytomegalovirus (CMV) infection (*27, 46*). Multiple putative markers of NK cell memory during
128 *Mtb* infection have been suggested, including CD57, CD8α, CD161, and CD27 (*28, 34, 45*). We
129 compared expression of these markers across clinical groups and found that household-associated
130 LTBI (IGRA+ contacts) and active TB disease donors had progressively decreasing frequency of
131 $CD8\alpha^{+}CD56^{dim}$ NK cells (**Fig. 4A)**. A similar trend was observed with the marker of terminal
132 differentiation, CD57. There was significantly fewer $CD57^{+}CD56^{dim}$ NK cells in household-
133 associated LTBI (IGRA+ contacts) compared to healthy household contacts (**Fig. 4B**). There was

134 no association between CD8α expression and age or sex, and loss of CD8α$^+$ was specific to NK
135 cells and was not observed among T cells during active TB (**Fig. S2A-B**). We did not observe any
136 significant differences in the expression of CD27, CD127, or CD161 between clinical groups (**Fig**
137 **S3**). Together, these results indicate that donors who develop household-associated LTBI and
138 active TB disease experience a loss of circulating CD8α$^+$ and CD57$^+$ CD56^{dim} NK cells. In turn,
139 CD8α$^+$ NK cell frequency significantly correlates with resistance to primary household-associated
140 infection.

141 **CD8α$^+$ NK cells represent a mature population with high functional potential:**

142 Despite the identification of cytotoxic CD8α$^+$ NK cells over 30 years ago (*47-49*), the function of
143 CD8α on NK cells during health and disease is not well-characterized and is of emerging interest
144 as a cellular target against immune-mediated diseases (*47, 49, 50*). We next used flow cytometry
145 to define co-expressed receptors of CD8α$^+$ NK cells in our cohorts. In the Haitian cohorts, a mean
146 of 27% of NK cells expressed CD8α on their surface. Among NK cell subsets, CD56^{dim} NK cells
147 had the largest proportion of CD8 positivity (median: 36%, range: 1-74%) (**Fig. S4A**). We then
148 defined co-expressed receptors on CD8α$^+$ NK cells among all healthy Haitian donors, excluding
149 active TB cases with chronic symptomatic disease. CD8α$^+$ NK cells expressed significantly higher
150 levels of CD57 and CD16, and lower levels of CD25 and CD127 (**Fig. 4C**). This indicates that
151 CD8α$^+$ NK cells represent more mature effectors compared to their CD8α$^-$ counterparts. When
152 compared to T cells, median fluorescence intensity (MFI) of CD8α surface expression was
153 significantly lower in NK cells (**Fig. S4B**).

154 To interrogate function, PBMCs were co-incubated with K562 cells for 15 hours and compared to
155 resting conditions as described above, stratified by CD8α. CD8α$^+$ NK cells were more responsive

156 to K562 induction measured by CD69 upregulation compared to CD8α$^-$ NK cells but demonstrated
157 lower levels of degranulation as measured by CD107a staining (**Fig. 4D**). The propensity for
158 CD8α$^+$ NK cells to upregulate CD69 upon K562 stimulation was more pronounced among the
159 CD56$^-$ compartment, where the CD8α$^-$ fraction had little to no response (**Fig. 4E**). Overall, this
160 suggests that CD8α expression among NK cells marks a population with higher capacity for
161 activation, specifically among terminally differentiated CD56$^-$ NK cells, that are reported to have
162 depressed effector functions (*51*).

163 **CD8α is ubiquitously expressed in NK cells:**

164 We next interrogated the immune phenotype and function of CD8α$^+$ NK cells in a distinct
165 biorepository of healthy human PBMCs (IRB2021-00478; PI: Vorkas) to validate our findings and
166 perform additional functional assays. First, we confirmed the presence of CD8α expression in NK
167 cells by extracellular staining with CD8α and CD8β antibodies. About 60% of NK cells did not
168 express surface CD8, CD8αα was found in ~40% of NK cells, while rare CD8αβ NK cells were
169 detected (**Fig. 5A**). In blood, CD8α was expressed in all three compartments of NK cells, and most
170 frequently among CD56^{dim} cells, with median expression comparable to Haitian donors (**Fig. 5B**).
171 We also validated our prior result from the contact cohort (**Fig. 4C**) demonstrating CD16 and
172 CD8α were significantly co-expressed (**Fig. 5C).** As our TB contact studies only assessed surface
173 CD8α on NK cells, we next analyzed intracellular CD8α expression by flow cytometry. We
174 observed that nearly all CD56^{dim} NK cells expressed CD8α protein intracellularly, contrasting with
175 T cells whose CD8 expression did not significantly differ between surface and intracellular
176 staining (**Fig. 5D**). CD56^{bright} and CD56$^-$ NK cells also demonstrated ubiquitous expression of
177 CD8α protein intracellularly (**Fig. S5**). To test the stability of surface CD8α on NK cells over time,

178 we incubated PBMCs for 1 or 7 days in pro-survival cytokine IL-2. We observed significantly
179 increased CD8α surface expression following prolonged incubation, indicating that surface
180 presentation of NK cell CD8α is more dynamic than in T cells where it is a constitutively expressed
181 surface receptor (**Fig. 5E**).

182 **CD8α$^+$ NK cells have enhanced responses to cytokine stimulation:**

183 We next hypothesized that surface CD8α was associated with enhanced responsiveness to
184 inflammatory signals, following prior reports of increased cytotoxicity against leukemic cells
185 relative to CD8α$^-$ NK cells (*48*). We stimulated PBMCs with either the potent IL15-IL15Rα sushi
186 domain fusion construct (IL15-15RαSu) (*52*), IL15-15RαSu/IL12/IL18, IL12/IL18 alone, or
187 virulent *Mtb* Erdman whole cell lysate and assessed intracellular IFNγ expression by flow
188 cytometry. Cytokine stimulation led to decreased CD8α$^+$ surface staining while *Mtb* stimulation
189 did not alter CD8 surface expression, suggesting that cytokine stimulation induces downregulation
190 of the CD8α receptor or cell death (**Fig. 6A**). Both IL15/IL12/IL18 and to a lesser degree *Mtb*
191 lysate conditions induced IFNγ responses in CD56^{dim} NK cells compared to resting (**Fig. 6B**).
192 When stratified by CD8α, we observed increased intracellular IFNγ with cytokine stimulation in
193 both CD16$^{-/+}$ CD8α$^+$ NK cells relative to CD8α$^-$ cells, but no differences upon co-incubation with
194 *Mtb* lysates (**Fig. 6C**). Percentage of CD25, CD69, and intracellular Granzyme B responses were
195 also enhanced in CD8α$^+$ NK cells across CD56-stratified subsets (**Fig. S6**).

196 **CD8α$^+$ surface expression on NK cells is MHC I-dependent:**

197 To determine a mechanism by which CD8α may modulate NK cell function, we hypothesized that
198 CD8α may engage MHC I molecules like CD8$^+$ T cells (*53, 54*). To test this, we stimulated whole
199 PBMCs with MHC I blocking antibody (clone: W6/32) and measured surface CD8α expression.

200 Strikingly, surface CD8α expression on NK cells—but not T cells—was significantly decreased
201 in all anti-MHC I conditions (**Fig. 6D**). Our results indicate that CD8α surface expression is
202 maintained through engagement of MHC I molecules.

203 **CD8α$^+$ NK cells have overlapping transcriptomes with CD8α$^-$ NK cells:**

204 While CD8α-expressing NK cells have previously been described (*47-49, 55*), the transcriptional
205 programs associated with surface expression of CD8α and whether these relate to homologous
206 function in CD8α$^+$ T cells during disease is an area of emerging interest. To interrogate the
207 transcriptional profile of CD8α$^+$ NK cells, we sorted innate lymphocyte subsets from PBMCs
208 including NK cells, γδ T cells, MAIT cells, and invariant Natural Killer T cells (iNKTs) by
209 fluorescence-activated cell sorting (FACS) from the peripheral blood of two healthy donors. We
210 performed CITE-seq (*7*) of these populations directly after sorting or after coincubation for seven
211 days in IL2/IL7 supplemented media +/- *Mtb* lysates in order to define surface protein and
212 transcript expression in CD8α NK cells. We discriminated NK cells from surrounding innate
213 lymphocytes based on surface antibody barcodes for CD56 and CD16 together with expression of
214 canonical NK cell gene transcripts *CD3E*, *NCR1*, and *NCAM1* (CD56) (**Fig. S7**) (*47, 56, 57*).
215 Dimensionality reduction with UMAP identified four clusters of NK cells with distinct
216 transcriptional signatures (**Fig. 7, A to D**). To assess pathogen-specific responses, we first
217 performed differential expression between the 'rest' and '*Mtb* lysate' conditions and display the
218 top 8 most differentially expression genes in **Fig. 7E**. The cytotoxic serine protease *GZMB*
219 *(*Granzyme B*)* and killer immunoglobulin-like receptor, *KIR3DL1*, were the most upregulated
220 genes in the *Mtb* lysate condition.

221 We next analyzed the distribution of *CD8A* transcript and CD8α protein expression among NK
222 cells using both transcript and surface antibody barcodes for CD8α. NK cells did not cluster
223 independently based on the presence of *CD8A*/CD8α (**Fig. 8, F and G**) and *CD8A*$^+$/CD8α$^+$ NK
224 cells were distributed throughout all clusters (**Fig. 8I)**. Low amplification of surface antibody
225 barcodes for CD8α was observed in NK cells, in contrast with other CD8α -expressing immune
226 subsets sequenced (e.g., MAIT cells; **Fig. S8**) in line with CD8α MFI differences detected by flow
227 cytometry (**Fig. S4B**).

228 To define transcriptional signatures associated with *CD8A* transcript expression, we stratified NK
229 cells expressing greater than zero *CD8A* transcripts and performed differential expression relative
230 to *CD8A*$^-$ cells. Half of all NK cells expressed *CD8A* transcripts (**Fig. 8J**). Differential gene
231 expression revealed few statistically significant differences between *CD8A*$^{+/-}$ cells. Notable
232 differentially expressed genes in *CD8A*$^+$ NK cells include cytotoxicity-associated proteins natural
233 cytotoxicity receptor 3 (*NCR3*) and the serine protease granzyme M (*GZMM*) (**Fig. 8K**).

234 **DISCUSSION**

235 Identifying the correlates of protection against natural *Mtb* infection is an area of critical
236 importance that will inform the next generation of TB vaccines and host-directed therapies (*5, 37,*
237 *45, 58-61*). In this study, we hypothesized that investigation of household-associated *Mtb* exposure
238 would reveal specialized NK cell populations and represent early events following high-risk
239 transmission. Our results identify a CD8α-expressing NK cell subpopulation with preserved
240 frequency in the blood of contacts who remain uninfected (IGRA-) that is progressively depleted
241 during household LTBI and active TB disease. Few studies have interrogated CD8α$^+$ NK cells, as
242 this receptor is most commonly understood as a lineage marker for T cells (*62*) and is absent in
243 specific pathogen free murine NK cells (*63*). Recent work reporting an association of CD8α$^+$ NK

244 cells with protection against human infectious, autoinflammatory and malignant disease has
245 generated interest in targeting this subpopulation for host-directed therapeutics (*39, 47, 48*).
246 However, little is known how CD8α receptors may modulate NK cell activity, namely, enhanced
247 cytotoxic functions previously reported in vitro against leukemia cells and strong associations with
248 protection against both infectious and non-infectious diseases. (*48, 50, 55*). Here, we show that the
249 majority of peripheral blood NK cells can express CD8α protein, but neither *CD8A* transcript nor
250 CD8α protein marked a distinct transcriptional state in healthy donors. Importantly, we
251 demonstrate that surface expression of CD8α on NK cells depends upon MHC I expression and
252 marks a population with enhanced responsiveness to cytokine stimuli in vitro. Together, our study
253 highlights a novel innate effector against human tuberculosis and provides important insights into
254 NK cell biology and innate TB immunology.

255 To our knowledge, there have been only two published household TB contact studies that
256 specifically examined NK cell biology during early *Mtb* exposure and infection. Our study expands
257 upon the sample size of this prior work and provides additional analyses of NK cell subpopulations
258 stratified by CD56 not previously addressed (*42, 64, 65*). Specifically, we observed decreased
259 frequency of immature $CD56^{bright}$ NK cells with reciprocal increase in mature $CD56^{-}$ NK cells
260 during community LTBI, in line with findings during chronic viral infections such hepatitis C and
261 HIV (*66-68*). We also observed that CD16 expression was increased during community LTBI
262 relative to household-associated infection, which may represent a late effect of latency within the
263 $CD56^{dim}$ subset (*61*). An equally valid interpretation of these results is that loss of surface CD16
264 is an early event detected after household-associated exposure and may represent downregulation
265 or shedding of the $F_c\gamma$ receptor after engagement (*40*). Together, these changes in frequency of
266 CD16 and CD56 expression indicate a gradual expansion of mature NK cells in peripheral blood

267 after asymptomatic infection (*29, 40, 64, 65, 67, 69*), accompanied by both markers of maturity
268 and dysfunction (loss of CD56), but also enhanced potential for ADCC (gain of CD16).

269 Two phenotypic markers whose surface expression were both independently and inversely
270 associated with infection in households, were CD8α and CD57. CD8α has long been appreciated
271 to be expressed on the surface of human (*47-50, 70*) and non-human primate NK cells (*63, 71*).
272 CD8α expression on human NK cells has been associated with enhanced cytotoxicity (*48, 55*) and
273 is referred to in one study as a putative *Mtb* memory marker (*45*). Recent studies in prospective
274 longitudinal human cohorts report that loss of CD8α expression at the transcript (*CD8A*) or protein
275 level correlate with HIV progression (*39, 49*), relapsing multiple sclerosis (*47*), and recurrence of
276 acute myeloid leukemia after stem cell transplantation (*50*), where CD8α$^+$ NK cells are
277 hypothesized to exercise combined cytotoxic and regulatory roles to prevent disease. Sorted
278 surface CD8α$^+$ NK cells also demonstrate enhanced anti-leukemia cytotoxicity in vitro compared
279 to sorted CD8α$^-$ cells (*50*). We also report that CD8α$^+$ NK cells were prevalent in healthy US
280 donors with ubiquitous intracellular CD8α protein expression. This finding suggests that most NK
281 cells are capable of presenting CD8α to the cell surface to enhance effector function, in contrast
282 to constitutive surface CD8α expression on T cells. Moreover, CD8α$^+$ NK cells were exquisitely
283 sensitive to cytokine stimulation, suggesting complex roles during inflammatory immune
284 responses against disease. Further, we show that CD8α surface expression was strongly dependent
285 on MHC I expression (*50, 54, 72*) raising critical questions for future studies to define the
286 molecular mechanisms of CD8α engagement with MHC I and to determine whether this may be
287 modulated by different peptide-MHC I complexes. Taken together with previously published work

288 (*47-49*), CD8α$^+$ NK cell subpopulations emerge as an attractive target in vaccination and host-
289 directed approaches against infectious and noninfectious diseases (*73*).

290 In addition to these mechanistic insights, we present the first multi-omic analysis of CD8α$^+$ NK
291 cells and show that in contrast to T cells, CD8α does not mark a distinct transcriptional state of
292 NK cells in healthy donors assayed, though *CD8A*$^+$ NK cells did differentially express cytotoxic
293 genes including *NCR3* and *GZMM*. These results will need to be validated in other healthy donors
294 as well as compared to future CITE-seq experiments in high-risk *Mtb* exposure cohorts or other
295 disease states.

296 There are certain limitations inherent to our human immunology study design. While household
297 contacts experienced high risk exposures to pre-treatment smear+ active TB cases, this does not
298 exclude the possibility they may have been exposed or infected in the community. We control for
299 this using source community donors to account for background transmission. Similarly, IGRA-
300 community controls may have also been recently exposed and resisted primary infection, though
301 this group represents the most rigorous control for household exposure. Our study was conducted
302 in one TB endemic population in Haiti and will need to be validated in other cohorts. Due to the
303 largely cross-sectional study design, we were unable to follow study volunteers beyond 6 months
304 for IGRA- contacts, of whom only two converted to IGRA+ providing insufficient sample size to
305 analyze correlates of IGRA conversion prospectively. Finally, all our biological samples in TB
306 cohorts were derived from human blood and may not represent the abundance or function of NK
307 cells within infected lung tissue. Future studies in *Mtb*-infected donors with multi-omic validation
308 are needed to understand the role of CD8α$^+$ NK cells at primary sites of infection.

309 In sum, our study adds to the growing literature highlighting a protective role for CD8α$^+$ NK cells
310 against both infections and non-infectious immune-mediated disease. Ongoing work will define

311 how surface CD8αα$^+$ NK cells may enhance targeting of *Mtb*-infected cells and will inform future
312 cellular therapies and vaccination approaches to prevent or treat TB disease.

313 **MATERIALS AND METHODS**

314 **Study design and participant recruitment:**

315 *Donor recruitment and protection of human subjects.* Haitian donors were enrolled through the
316 Tri-Institutional Tuberculosis Research Unit (TBRU) at the Groupe Haitien d'etude du Sarcome
317 de Kaposi et des Infections Opportunistes (GHESKIO) Centers under Institutional Review Board
318 Approval at Weill Cornell Medicine and GHESKIO Centers in Haiti. All participants provided
319 written informed consent, including consent for future use of biobanked samples for research. A
320 dedicated clinical field team at the GHESKIO Centers in Port-au-Prince, Haiti, recruited as part of
321 the NIH-funded TBRU (AI111143). LTBI was detected using QuantiFERON-TB® Gold
322 (QIAGEN), and active TB was excluded by clinical screening for signs and symptoms of active
323 TB including fever, cough, night sweats, weight loss, and abnormal findings on Chest X-ray. Most
324 contacts were recruited close to the time of diagnosis of the index case and were living in the same
325 house as the active TB case for at least 1 month in the 6 months prior to diagnosis (median time to
326 contact recruitment from TB case diagnosis, 2.4 months; range, 0.2-26 months). To select for high
327 transmission settings, each household was required to have a history of two active pulmonary TB
328 cases. Healthy donors without reported TB exposure from the same community were recruited as
329 controls. All cases with active pulmonary TB received periodic follow-up appointments while on
330 treatment, and anyone with known contact with an active TB patient who remained IGRA-
331 received 6-month follow-up and was rescreened with IGRA. The median smear grade of the active
332 pulmonary TB cases in the households was 2-3+, conferring high risk for person-to-person
333 transmission (*74*). All donors provided informed consent prior to peripheral blood donation for

334 PBMC isolation. All donor samples were de-identified on site using a barcode system before they
335 were shipped to Stony Brook University for analysis. Healthy donors were also recruited at Stony
336 Brook University (SBU) under IRB2021-00478 (PI: Vorkas) and New York Blood Center
337 (NYBC), which were used for stimulation assays and CITE-seq.

338 **PBMC isolation:**

339 PBMCs were isolated from peripheral blood at GHESKIO (Port-au-Prince, Haiti) using the Ficoll-
340 Paque (GE Healthcare) density centrifugation, frozen in 5×10^6 cells/ml aliquots in 90% FBS/10%
341 DMSO (Thermo Fisher Scientific) and stored at –80°C prior to being shipped on dry ice to New
342 York. PBMCs from healthy donors recruited at SBU and New York Blood Center (NYBC) were
343 isolated using Ficoll-Paque, BD Vacutainer CPT cell preparation tube (Becton, Dickinson and
344 Company) or SepMate tubes (Stem Cell Technologies) using the manufacturer protocol. PBMCs
345 isolated at SBU were cryopreserved in serum free Bambanker medium (GC Lymphotec) and stored
346 in liquid N_2.

347 **Flow cytometry acquisition and analysis:**

348 A complete list of fluorescent antibodies is listed in Supplementary Table 1: Reagents and
349 resources. All antibodies were commercially acquired, and multicolor panels were designed and
350 validated using fluorescent minus one (FMO) controls. MR1 tetramers were obtained from the
351 NIH Tetramer Core Facility (Atlanta, GA). In brief, cryopreserved PBMCs were thawed, plated,
352 Fc receptor blocked (eBioscience), and underwent direct ex vivo extracellular staining for 15
353 minutes at room temperature (RT). For intracellular staining, PBMCs were incubated with 1X
354 Brefeldin A (BioLegend) for final hour of incubation prior to staining with intracellular antibodies.
355 Samples were then washed twice with FACS buffer and acquired using an Aurora Spectral
356 Analyzer (Cytek). Flow cytometry analysis, including manual gating, was performed using FCS

357 Express 7 (De Novo Software) or R (v4.3.1) with the following library packages downloaded from
358 Bioconductor: *flowWorkspace, ggcyto, and flowCore*.

359 ***Mtb* whole cell lysate:**

360 *Mtb* whole cell lysate was prepared in Biosafety Level 3 facility at SBU. Fifty mL of *Mtb* Erdman
361 7H9 culture was grown to OD_{600} 0.6, centrifuged at 4000 × g for 10 min at RT and pellet was
362 resuspended in 2.5 ml of 10mM Tris-HCl buffer (pH 7.5) and rotated for 2 hr at RT. The mixture
363 was centrifuged at 500 × g for 15 min at RT and aqueous phase was collected and filtered twice
364 through 0.22 µM spin filter (Corning Costar Spin-X) at 6000 × g for 5 min. The aliquots were
365 stored at -80°C for further use.

366 **NK cell co-culture with K562 cell line**

367 K562 cells (ATCC) were incubated in Iscove's Modified Dulbecco's Medium (IMDM)
368 supplemented with 10% FBS. Cryopreserved K562 cells were thawed at 37°C water bath and cells
369 were cultured at 1 x 10^5 viable cells/ml in T-75 flask as per manufacturers protocol. Once the cell
370 density reached 1 x 10^6 cells/ml, K562 was co-incubated with PBMCs at 1:20 K562 to PBMC in
371 a round bottom clear plate (Greiner) for 15 hrs, at 37°C with 5% CO_2. At the beginning of
372 incubation period anti-CD107a antibody was added to the culture. After incubation was complete,
373 cells were washed, stained and acquired by flow cytometry.

374 **NK cell stimulation assay:**

375 Cryopreserved healthy donor PBMCs from SBU and NYBC were used for NK cell stimulation
376 assays. Thawed PBMCs were cultured 1 x 10^4 cells per well in round bottom clear plate (Greiner)
377 for 15 hr, at 37°C with 5% CO_2. Samples were stimulated and incubated overnight in complete
378 RPMI media with 10% heat-inactivated FBS and supplemented with IL-2 (50 U/ml; PeproTech).

379 The cytokine stimulation conditions were performed with commercially available recombinant IL-
380 12 (100 ng/mL; BioLegend), recombinant IL-18 (100 ng/mL; Biolegend) and IL15-Su construct
381 (1 µg/ml) containing a truncated Sushi domain of IL15Rα synthesized by the Cheung lab, that is
382 demonstrated to be a more potent and stable compound with longer half-life than recombinant
383 IL15 (*52*). For *Mtb* stimulation condition we used 1:100 and 1:200 dilution of *Mtb* whole cell
384 lysate.

385 **MHC I blockade:**

386 Cryopreserved healthy donor PBMCs from SBU and NYBC were used for MHC I blockade.
387 PBMCs were thawed at 37°C and incubated in complete RPMI media with 10% heat-inactivated
388 FBS and supplemented with IL-2 (50 U/ml; PeproTech). 1 x 10^4 PBMCs were plated per well in
389 round bottom clear plate (Greiner) and incubated with or without 5 µg/ml *Invivo*MAb anti-human
390 MHC I (clone W6/32; Bio X cell) for 15 hr, at 37°C with 5% CO_2 before being stained and
391 acquired.

392 **scRNA-seq and CITE-seq library generation and sequencing:**

393 PBMCs were stained with fluorescent antibodies for cell sorting of MAIT cells ($CD3^+$, $CD161^+$,
394 MR1-5-OP-RU $tetramer^+$), NK cells ($CD3^-$, $CD19^-$, $CD14^-$, $CD16^+$ $CD56^{dim}$), γδ T cells ($CD3^+$,
395 $TCR\gamma\delta^+$) and iNKT cells ($CD161^+$ $iNKT^+$) using FACS. The sorted cells were blocked with human
396 Trustain, FcX blocking reagent (BioLegend) for 10 minutes at 4ºC and then stained with TotalSeq-
397 C barcoded tagged and hashtags antibodies for 30 minutes at 4ºC in a total volume of 100ul. The
398 residual TotalSeq-C and hashtags antibodies were removed by centrifugation at 400 *g* for 5
399 minutes at 4ºC. A complete hashtag and TotalSeq-C antibody list is provided in **Supplementary**
400 **Table 1: Reagent and Resources.**

401 Gene expression and surface antigen library preparation was conducted at the Stony Brook
402 University Single Cell Genomics Facility. Briefly, cell viability and concentrations were
403 determined on a Countess 3FL with trypan blue staining. Approximately 5,000 live cells from each
404 condition were loaded in a single 10X Genomics 5' NextGEM Single Cell assay reaction (30,000
405 total cells per reaction), to perform 5' single cell immune profiling assay using a Chromium iX
406 instrument (10X Genomics). Gene expression (GEX) and surface antigen (SA) libraries were
407 prepared, and quality controlled using Chromium NextGEM 5' Single Cell with Feature Barcode
408 assay and a TapeStation 4200, according to the manufacturer's instructions. The libraries were
409 sequenced at a depth of approx. 25,000 (GEX) and 10,000 (SA) paired reads/cell on an Illumina
410 NovaSeqX sequencer (Novogene, Inc).

411 The gene expression and surface feature barcode raw FASTQ files of single cell RNA-seq were
412 analyzed on Cell Ranger (10x Genomics, v.7.0) (https://www.10xgenomics.com/analysis-
413 guides/demultiplexing-and-analyzing-5%E2%80%99-immune-profiling-libraries-pooled-with-
414 hashtags), multi-pipeline with human reference transcriptome (GRCh38) downloaded from 10x
415 Genomics website and hashtag configuration file, which contained the barcodes related to each
416 different samples.

417 **Single-cell RNAseq analysis:**

418 The generated gene expression matrix files were analyzed with R (4.3.2) using the *Seurat* (5.0)
419 package and cells were filtered based on following criteria: 1.) the number of genes was equal to
420 or greater than 200 and below than 6000 and 2.) the mitochondrial percentage was less than 5.
421 Using the FindVariableFeatures() function we selected the top 3000 features with highest variance.
422 Then, different samples were integrated using the harmony algorithm and scaled. Log-
423 normalization and principal component analysis (PCA) was done on integrated values. The top 20

424 principal components were selected for clustering and visualization with UMAP using the default
425 Louvain algorithm. Differential gene expression was performed using FindAllMarkers() with a
426 minimum threshold of 25% cells expressing.

427 **Statistical Analysis:**

428 Statistical analysis was performed using R (4.3.2) and GraphPad Prism (10.1.2). Non-parametric
429 testing with Wilcoxon tests was used to compare the means between groups for flow markers. P-
430 values were not adjusted because cross-wise comparisons were not performed between all six
431 clinical groups. Only comparisons a priori hypothesized to represent biological features were
432 tested, these included: IGRA- contacts vs controls, IGRA+ contacts vs controls, IGRA- contact vs
433 IGRA+ control, and IGRA+ control vs Active TB.

434 **Supplementary Materials**

435 Supplementary Table 1: Reagents and resources. See attached file.

436 **References and Notes:**

437 1. R. M. Houben, P. J. Dodd, The Global Burden of Latent Tuberculosis Infection: A Re-
438 estimation Using Mathematical Modelling. *PLoS Med* **13**, e1002152 (2016).
439 2. S. Bagcchi, WHO's Global Tuberculosis Report 2022. *Lancet Microbe* **4**, e20 (2023).
440 3. K. M. Shea, J. S. Kammerer, C. A. Winston, T. R. Navin, C. R. Horsburgh, Jr., Estimated
441 rate of reactivation of latent tuberculosis infection in the United States, overall and by
442 population subgroup. *Am J Epidemiol* **179**, 216-225 (2014).
443 4. K. B. Urdahl, S. Shafiani, J. D. Ernst, Initiation and regulation of T-cell responses in
444 tuberculosis. *Mucosal Immunol* **4**, 288-293 (2011).

445 5. E. Nemes *et al.*, Prevention of M. tuberculosis Infection with H4:IC31 Vaccine or BCG
446 Revaccination. *N Engl J Med* **379**, 138-149 (2018).
447 6. D. R. Tait *et al.*, Final Analysis of a Trial of M72/AS01E Vaccine to Prevent Tuberculosis.
448 *N Engl J Med* **381**, 2429-2439 (2019).
449 7. A. Nathan *et al.*, Multimodally profiling memory T cells from a tuberculosis cohort
450 identifies cell state associations with demographics, environment and disease. *Nat Immunol*
451 **22**, 781-793 (2021).
452 8. A. Pradhan, C. K. Vorkas, T cells target TB. *Cell Host Microbe* **31**, 329-330 (2023).
453 9. A. M. Gallegos *et al.*, A gamma interferon independent mechanism of CD4 T cell mediated
454 control of M. tuberculosis infection in vivo. *PLoS Pathog.* **7**, e1002052 (2011).
455 10. S. Sakai *et al.*, CD4 T Cell-Derived IFN-gamma Plays a Minimal Role in Control of
456 Pulmonary Mycobacterium tuberculosis Infection and Must Be Actively Repressed by PD-
457 1 to Prevent Lethal Disease. *PLoS Pathog.* **12**, (2016).
458 11. H. A. Fletcher, L. Schrager, TB vaccine development and the End TB Strategy: importance
459 and current status. *Trans R Soc Trop Med Hyg* **110**, 212-218 (2016).
460 12. G. Voss *et al.*, Progress and challenges in TB vaccine development. *F1000Res* **7**, 199
461 (2018).
462 13. J. D. Ernst, Mechanisms of M. tuberculosis Immune Evasion as Challenges to TB Vaccine
463 Design. *Cell Host Microbe* **24**, 34-42 (2018).
464 14. D. Roordink *et al.*, The TB vaccine development pathway - An innovative approach to
465 accelerating global TB vaccine development. *Tuberculosis (Edinb)* **126**, 102040 (2021).
466 15. C. K. Vorkas *et al.*, Mucosal-associated invariant and gammadelta T cell subsets respond
467 to initial Mycobacterium tuberculosis infection. *JCI Insight* **3**, (2018).

468 16. J. A. Choreno-Parra, L. I. Weinstein, E. J. Yunis, J. Zuniga, R. Hernandez-Pando, Thinking
469 Outside the Box: Innate- and B Cell-Memory Responses as Novel Protective Mechanisms
470 Against Tuberculosis. *Front Immunol* **11**, 226 (2020).
471 17. S. A. Khader *et al.*, Targeting innate immunity for tuberculosis vaccination. *J Clin Invest*
472 **129**, 3482-3491 (2019).
473 18. J. A. Choreño Parra *et al.*, Memory of Natural Killer Cells: A New Chance against
474 Mycobacterium tuberculosis? *Front Immunol* **8**, 967 (2017).
475 19. D. Artis, H. Spits, The biology of innate lymphoid cells. *Nature* **517**, 293-301 (2015).
476 20. P. Dogra *et al.*, Tissue Determinants of Human NK Cell Development, Function, and
477 Residence. *Cell* **180**, 749-763.e713 (2020).
478 21. L. L. Lanier, Natural killer cell receptor signaling. *Current opinion in immunology* **15**, 308-
479 314 (2003).
480 22. P. Schierloh *et al.*, Mycobacterium tuberculosis-induced gamma interferon production by
481 natural killer cells requires cross talk with antigen-presenting cells involving Toll-like
482 receptors 2 and 4 and the mannose receptor in tuberculous pleurisy. *Infect Immun* **75**, 5325-
483 5337 (2007).
484 23. S. Venkatasubramanian *et al.*, IL-21-dependent expansion of memory-like NK cells
485 enhances protective immune responses against Mycobacterium tuberculosis. *Mucosal*
486 *Immunol* **10**, 1031-1042 (2017).
487 24. S. Esin, G. Batoni, Natural killer cells: a coherent model for their functional role in
488 Mycobacterium tuberculosis infection. *J Innate Immun* **7**, 11-24 (2015).
489 25. C. B. W. Giacoia-Gripp *et al.*, Changes in the NK Cell Repertoire Related to Initiation of
490 TB Treatment and Onset of Immune Reconstitution Inflammatory Syndrome in TB/HIV

491 Co-infected Patients in Rio de Janeiro, Brazil-ANRS 12274. *Front Immunol* **10**, 1800
492 (2019).
493 26. M. Allen *et al.*, Mechanisms of Control of Mycobacterium tuberculosis by NK Cells: Role
494 of Glutathione. *Front Immunol* **6**, 508 (2015).
495 27. M. Garand *et al.*, Functional and Phenotypic Changes of Natural Killer Cells in Whole
496 Blood during Mycobacterium tuberculosis Infection and Disease. *Front Immunol* **9**, 257
497 (2018).
498 28. L. D. Harris *et al.*, Distinct Human NK Cell Phenotypes and Functional Responses to
499 Mycobacterium tuberculosis in Adults From TB Endemic and Non-endemic Regions.
500 *Front Cell Infect Microbiol* **10**, 120 (2020).
501 29. G. Batoni *et al.*, Human CD56bright and CD56dim natural killer cell subsets respond
502 differentially to direct stimulation with Mycobacterium bovis bacillus Calmette-Guérin.
503 *Scand J Immunol* **62**, 498-506 (2005).
504 30. S. Esin *et al.*, Interaction of Mycobacterium tuberculosis cell wall components with the
505 human natural killer cell receptors NKp44 and Toll-like receptor 2. *Scand J Immunol* **77**,
506 460-469 (2013).
507 31. S. Esin *et al.*, Functional characterization of human natural killer cells responding to
508 Mycobacterium bovis bacille Calmette-Guérin. *Immunology* **112**, 143-152 (2004).
509 32. R. Vankayalapati *et al.*, Role of NK cell-activating receptors and their ligands in the lysis
510 of mononuclear phagocytes infected with an intracellular bacterium. *J Immunol* **175**, 4611-
511 4617 (2005).
512 33. R. Vankayalapati *et al.*, The NKp46 receptor contributes to NK cell lysis of mononuclear
513 phagocytes infected with an intracellular bacterium. *J Immunol* **168**, 3451-3457 (2002).

514 34. D. Tripathi *et al.*, Metabolites enhance innate resistance to human Mycobacterium
515 tuberculosis infection. *JCI Insight* **7**, (2022).
516 35. M. E. Ross, M. A. Caligiuri, Cytokine-induced apoptosis of human natural killer cells
517 identifies a novel mechanism to regulate the innate immune response. *Blood* **89**, 910-918
518 (1997).
519 36. W. E. Carson *et al.*, Interleukin (IL) 15 is a novel cytokine that activates human natural
520 killer cells via components of the IL-2 receptor. *J Exp Med* **180**, 1395-1403 (1994).
521 37. S. Suliman *et al.*, Peripheral Blood Mucosal-Associated Invariant T Cells in Tuberculosis
522 Patients and Healthy Mycobacterium tuberculosis-Exposed Controls. *J Infect Dis* **222**, 995-
523 1007 (2020).
524 38. P. Schierloh *et al.*, Increased susceptibility to apoptosis of CD56dimCD16+ NK cells
525 induces the enrichment of IFN-gamma-producing CD56bright cells in tuberculous
526 pleurisy. *J Immunol* **175**, 6852-6860 (2005).
527 39. B. Lucia, C. Jennings, R. Cauda, L. Ortona, A. L. Landay, Evidence of a selective depletion
528 of a CD16+ CD56+ CD8+ natural killer cell subset during HIV infection. *Cytometry* **22**,
529 10-15 (1995).
530 40. K. Srpan *et al.*, Shedding of CD16 disassembles the NK cell immune synapse and boosts
531 serial engagement of target cells. *J Cell Biol* **217**, 3267-3283 (2018).
532 41. I. Terren *et al.*, Cytokine-Induced Memory-Like NK Cells: From the Basics to Clinical
533 Applications. *Front Immunol* **13**, 884648 (2022).
534 42. D. Brownlie *et al.*, Expansions of adaptive-like NK cells with a tissue-resident phenotype
535 in human lung and blood. *Proc Natl Acad Sci U S A* **118**, (2021).

536 43. R. Nikzad *et al.*, Human natural killer cells mediate adaptive immunity to viral antigens.
537 *Sci Immunol* **4**, (2019).
538 44. N. M. Adams *et al.*, Cytomegalovirus Infection Drives Avidity Selection of Natural Killer
539 Cells. *Immunity* **50**, 1381-1390 e1385 (2019).
540 45. S. Suliman *et al.*, Bacillus Calmette-Guérin (BCG) Revaccination of Adults with Latent
541 Mycobacterium tuberculosis Infection Induces Long-Lived BCG-Reactive NK Cell
542 Responses. *J Immunol* **197**, 1100-1110 (2016).
543 46. K. Van Der Ploeg *et al.*, Emergence of Human CMV-induced NKG2C+ NK cells is
544 Associated with CD8+ T cell Recovery following Allogeneic HCT. *Blood Adv*, (2023).
545 47. E. F. McKinney *et al.*, A CD8(+) NK cell transcriptomic signature associated with clinical
546 outcome in relapsing remitting multiple sclerosis. *Nat Commun* **12**, 635 (2021).
547 48. E. G. Addison *et al.*, Ligation of CD8alpha on human natural killer cells prevents
548 activation-induced apoptosis and enhances cytolytic activity. *Immunology* **116**, 354-361
549 (2005).
550 49. F. Ahmad *et al.*, High frequencies of polyfunctional CD8+ NK cells in chronic HIV-1
551 infection are associated with slower disease progression. *J Virol* **88**, 12397-12408 (2014).
552 50. M. W. Lowdell *et al.*, Evidence that continued remission in patients treated for acute
553 leukaemia is dependent upon autologous natural killer cells. *Br J Haematol* **117**, 821-827
554 (2002).
555 51. N. K. Björkström, H.-G. Ljunggren, J. K. Sandberg, CD56 negative NK cells: origin,
556 function, and role in chronic viral disease. *Trends in Immunology* **31**, 401-406 (2010).
557 52. H. Xu, I. N. Buhtoiarov, H. Guo, N. V. Cheung, A novel multimeric IL15/IL15Rα-Fc
558 complex to enhance cancer immunotherapy. *Oncoimmunology* **10**, 1893500 (2021).

559 53. L. J. Walker *et al.*, Human MAIT and CD8alphaalpha cells develop from a pool of type-
560 17 precommitted CD8+ T cells. *Blood* **119**, 422-433 (2012).
561 54. H. Cheroutre, F. Lambolez, Doubting the TCR coreceptor function of CD8alphaalpha.
562 *Immunity* **28**, 149-159 (2008).
563 55. K. Kushima *et al.*, Flow cytometric analysis of chicken NK activity and its use on the effect
564 of restraint stress. *J Vet Med Sci* **65**, 995-1000 (2003).
565 56. M. Gutierrez-Arcelus *et al.*, Lymphocyte innateness defined by transcriptional states
566 reflects a balance between proliferation and effector functions. *Nat Commun.* **10**, 687
567 (2019).
568 57. C. Yang *et al.*, Heterogeneity of human bone marrow and blood natural killer cells defined
569 by single-cell transcriptome. *Nat Commun* **10**, 3931 (2019).
570 58. M. Musvosvi *et al.*, T cell receptor repertoires associated with control and disease
571 progression following Mycobacterium tuberculosis infection. *Nat Med*, (2023).
572 59. S. Suliman *et al.*, MR1-Independent Activation of Human Mucosal-Associated Invariant
573 T Cells by Mycobacteria. *J Immunol.* **203**, 2917-2927 (2019).
574 60. P. Andersen, T. J. Scriba, Moving tuberculosis vaccines from theory to practice. *Nat Rev*
575 *Immunol* **19**, 550-562 (2019).
576 61. R. Roy Chowdhury *et al.*, A multi-cohort study of the immune factors associated with M.
577 tuberculosis infection outcomes. *Nature* **560**, 644-648 (2018).
578 62. D. Masopust, V. Vezys, E. J. Wherry, R. Ahmed, A brief history of CD8 T cells. *Eur J*
579 *Immunol* **37 Suppl 1**, S103-110 (2007).
580 63. L. J. Kieffer *et al.*, Human CD8 alpha expression in NK cells but not cytotoxic T cells of
581 transgenic mice. *Int Immunol* **8**, 1617-1626 (1996).

582 64. B. Muller-Durovic, J. Grahlert, O. P. Devine, A. N. Akbar, C. Hess, CD56-negative NK
583 cells with impaired effector function expand in CMV and EBV co-infected healthy donors
584 with age. *Aging (Albany NY)* **11**, 724-740 (2019).
585 65. A. Poli *et al.*, CD56bright natural killer (NK) cells: an important NK cell subset.
586 *Immunology* **126**, 458-465 (2009).
587 66. A. S. Fauci, D. Mavilio, S. Kottilil, NK cells in HIV infection: paradigm for protection or
588 targets for ambush. *Nat Rev Immunol* **5**, 835-843 (2005).
589 67. N. K. Björkström, H. G. Ljunggren, J. K. Sandberg, CD56 negative NK cells: origin,
590 function, and role in chronic viral disease. *Trends Immunol* **31**, 401-406 (2010).
591 68. B. Rehermann, M. Nascimbeni, Immunology of hepatitis B virus and hepatitis C virus
592 infection. *Nat Rev Immunol* **5**, 215-229 (2005).
593 69. L. L. Lanier, R. Testi, J. Bindl, J. H. Phillips, Identity of Leu-19 (CD56) leukocyte
594 differentiation antigen and neural cell adhesion molecule. *J Exp Med* **169**, 2233-2238
595 (1989).
596 70. L. A. Terry, J. P. DiSanto, T. N. Small, N. Flomenberg, Differential expression and
597 regulation of the human CD8 alpha and CD8 beta chains. *Tissue Antigens* **35**, 82-91 (1990).
598 71. R. L. Webster, R. P. Johnson, Delineation of multiple subpopulations of natural killer cells
599 in rhesus macaques. *Immunology* **115**, 206-214 (2005).
600 72. J. Geng, M. Raghavan, CD8alphaalpha homodimers function as a coreceptor for
601 KIR3DL1. *Proc Natl Acad Sci U S A* **116**, 17951-17956 (2019).
602 73. S. Schmidt, L. Tramsen, B. Rais, E. Ullrich, T. Lehrnbecher, Natural killer cells as a
603 therapeutic tool for infectious diseases - current status and future perspectives. *Oncotarget*
604 **9**, 20891-20907 (2018).

605 74. H. del Corral *et al.*, IFNgamma response to Mycobacterium tuberculosis, risk of infection
606 and disease in household contacts of tuberculosis patients in Colombia. *PLoS One* **4**, e8257
607 (2009).

608 **Acknowledgments:** We are thankful for the support of the Stony Brook Foundation, the
609 Department of Medicine of the Renaissance School of Medicine and the Office of the Vice
610 President of Research of Stony Brook University. We thank Daniel W. Fitzgerald, MD
611 (Weill Cornell Medicine, Center for Global Health) and Michael S. Glickman (Memorial
612 Sloan Kettering Cancer Center) for generously providing clinical samples from TB contact
613 cohorts. We thank Joseph C. Sun (MSKCC) for valuable discussions on adaptive NK cells.
614 We are also grateful to Thomas MacCarthy, PhD (Stony Brook University, Applied
615 Mathematics) for supportive advice regarding CITE-seq analyses, who passed away during
616 the preparation of this manuscript.

617 **Funding:** This study was supported by the Tri-I TBRU, part of the TBRU Network (U19
618 AI11143). CKV acknowledges support from the NIAID T32 Pathogenesis of Infectious
619 Diseases Training Program (T32AI007613-18; Roy Gulick, WCM), the IDSA Education
620 and Research Foundation Postdoctoral Fellowship Award in Infectious Diseases, a Potts
621 Memorial Foundation Award, NIAID K08AI132739, R21AI171578, and R21AI183259.

622 **Author contributions:** The following authors contributed to the manuscript in various ways. Each
623 author's contribution is listed below.

624 Conceptualization: KH, JBL, CKV

625 Methodology: NKC, AP, RK, KCH, JBL, CKV

626 Investigation: NM, AP, RK, TK, BR, NKC, HX, JBL and CKV

Visualization: NM, AP, RK, JB, BR, DEC, JBL, and CKV

Funding acquisition: CKV

Writing – original draft: NM, AP, CKV

Writing – review & editing: all authors

Competing interests: Authors declare that they have no competing interests.

Data and materials availability: All data, code, and materials used in the analysis will be available to any researcher for purposes of reproducing or extending the analysis.

635 **Figures:**

Variable	Control (n=50)	Contact (n=50)	Active TB (n=50)
Age – yr	30.1 ± 9.3	33.9 ± 17.8	20.2 ± 4.26
≤ 18 yr	2 (4)	12 (24)	18 (36)
>18 and <65	48 (96)	35 (76)	32 (64)
≥ 65 yr	0 (0)	3	0 (0)
Female sex – no. (%)	26 (52)	30 (60)	26 (52)
IGRA positive – no. (%)	25 (50)	34 (68)	38 (76)

636 **Table 1. Demographics of study participants in Haitian Cohort (N=150)**

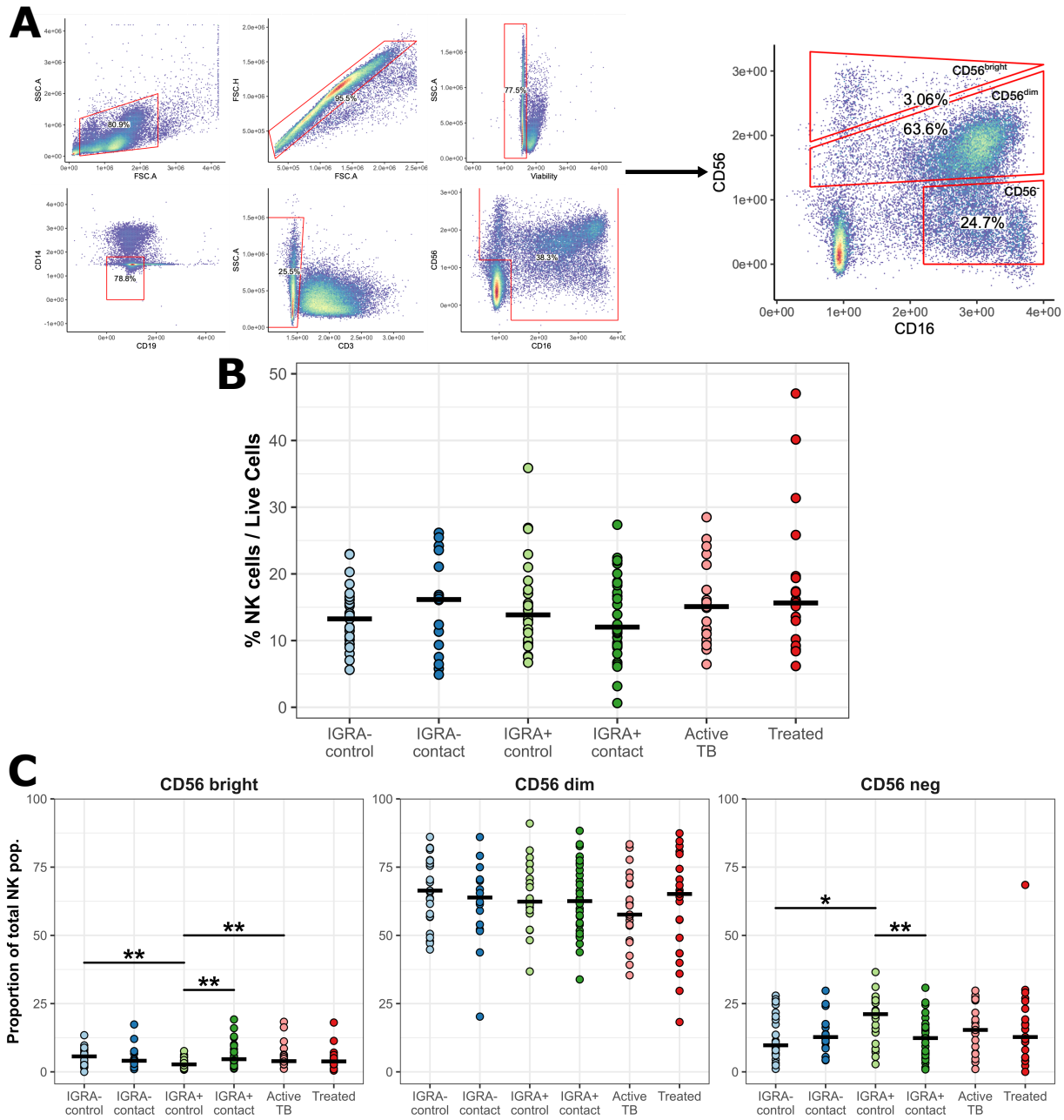

Fig. 1. Frequencies of NK cell subpopulations are altered after *Mtb* infection. (A) Gating strategy employed for NK cells from a representative sample. NK cells were defined as CD19$^-$, CD3$^-$, CD14$^-$ lymphocytes who expressed any level of either CD16 or CD56. NK cells were further subdivided into three subsets based on CD56 expression. **(B)** Change in frequency of total NK cells as a proportion of total live population. **(C)** Frequency of each NK cell subset in clinical groups. Frequency calculated as percent of each subset among total NK cells. Brackets represent Wilcoxon statistical tests, with unadjusted p-values. *$p \leq 0.05$, **$p \leq 0.01$.

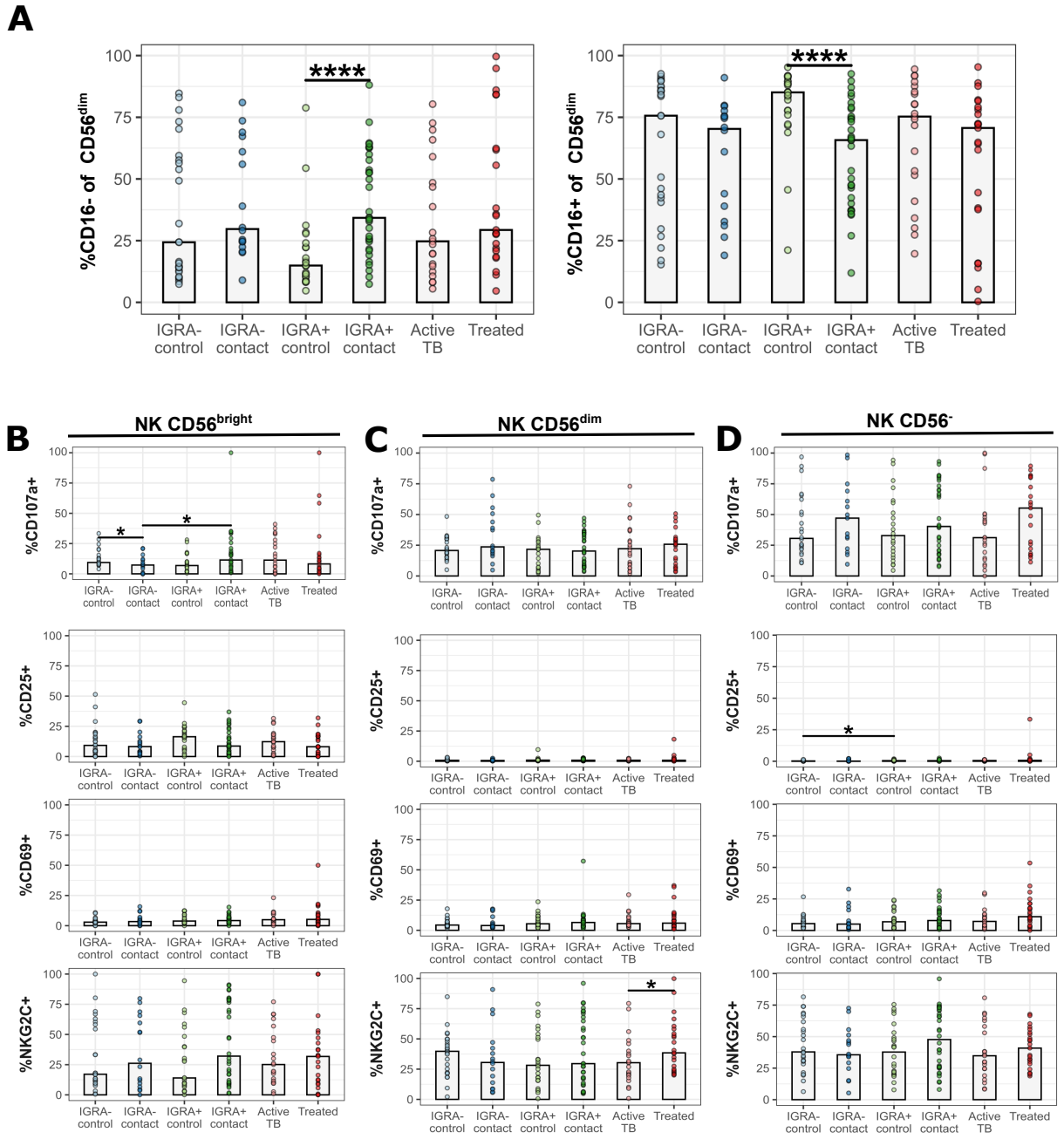

644 **Fig. 2. NK cells demonstrate loss of CD16 expression during household-associated latent infection. (A)**
645 Frequency of CD16 in CD56^{dim} NK cells. Brackets represent Wilcoxon tests with unadjusted p-values.
646 Percent positive for 5 activation markers in **(B)** CD56^{bright} NK cells, **(C)** CD56^{dim} NK cells, and **(D)**
647 CD56^{-} NK cells. Brackets represent Wilcoxon tests with unadjusted p-values. *$p \leq 0.05$, ****$p \leq$
648 0.0001.

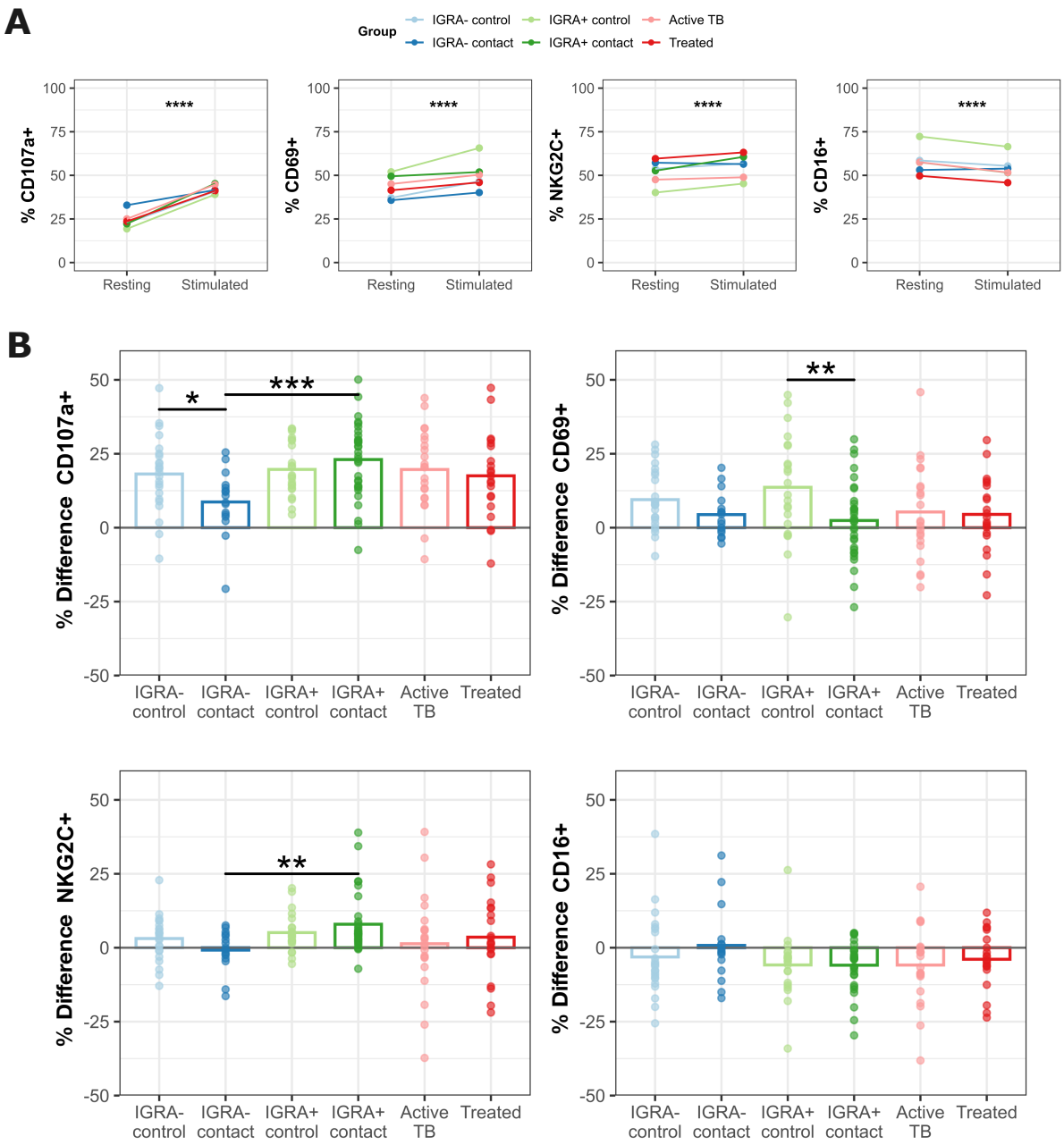

649 **Fig. 3. *Mtb* resistors demonstrate depressed NK cell function in vitro.** NK cells stimulated overnight by co-
650 culture with K562 cell line compared to plain media alone. **(A)** Overall results of activation assay for
651 $CD56^{dim}$ NK cells for four activation markers. Y-axis represents mean percent positive for each activation
652 marker. P values calculated as a global paired Wilcoxon test including all clinical groups. Each clinical
653 group is displayed separately indicated by line color. **(B)** Percent difference of four activation markers
654 (stimulated minus resting) comparing between clinical groups. Brackets represent Wilcoxon tests with
655 unadjusted p-values. *$p \leq 0.05$, **$p \leq 0.01$, ***$p \leq 0.001$, ****$p \leq 0.0001$.

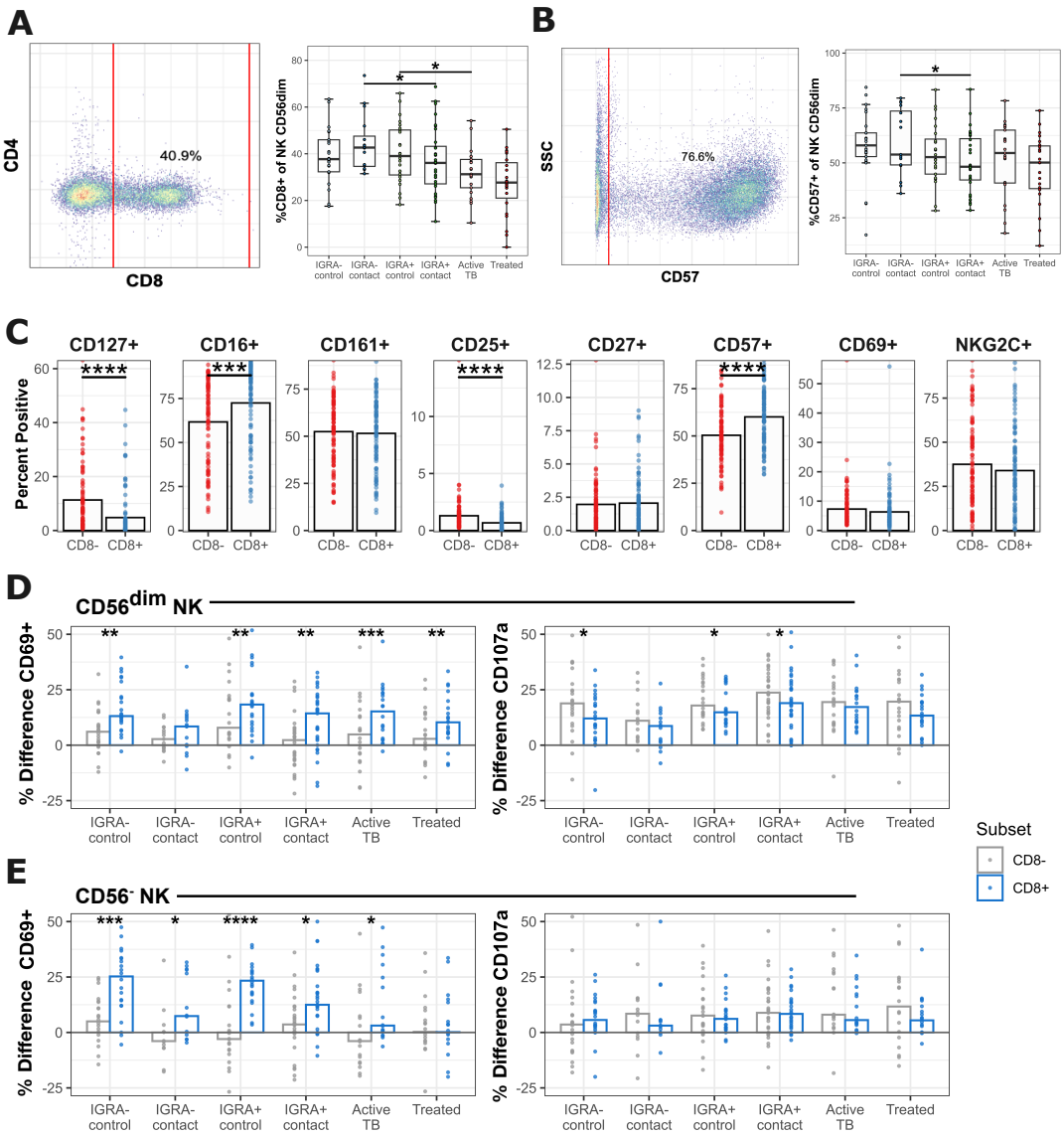

Fig. 4. CD8α$^+$ NK cells are depleted in the blood of cases with household-associated *Mtb* infection. (A) Representative gating of CD8α$^+$ in CD56^{dim} NK cells and frequency of CD8α$^+$ within CD56^{dim} NK cells. **(B)** Representative gating of CD57 in CD56^{dim} NK cells and boxplots of percent CD57$^+$ within CD56^{dim} NK cells. **(C)** Expression of select surface markers between CD8α$^+$ vs CD8α$^-$ CD56^{dim} NK cells, active TB are excluded. **(D)** Activation assay with overnight K562 co-culture versus plain media comparing CD8α$^+$ vs CD8α$^-$ CD56^{dim} NK cells. Y-values represent percent difference for CD69 and CD107a. Asterisks represent paired Wilcoxon tests. **(E)** As in panel D, instead displaying CD56$^-$ NK cells. P-values represent unadjusted Wilcoxon testing. *$p \leq 0.05$, **$p \leq 0.01$, ***$p \leq 0.001$, ****$p \leq 0.0001$.

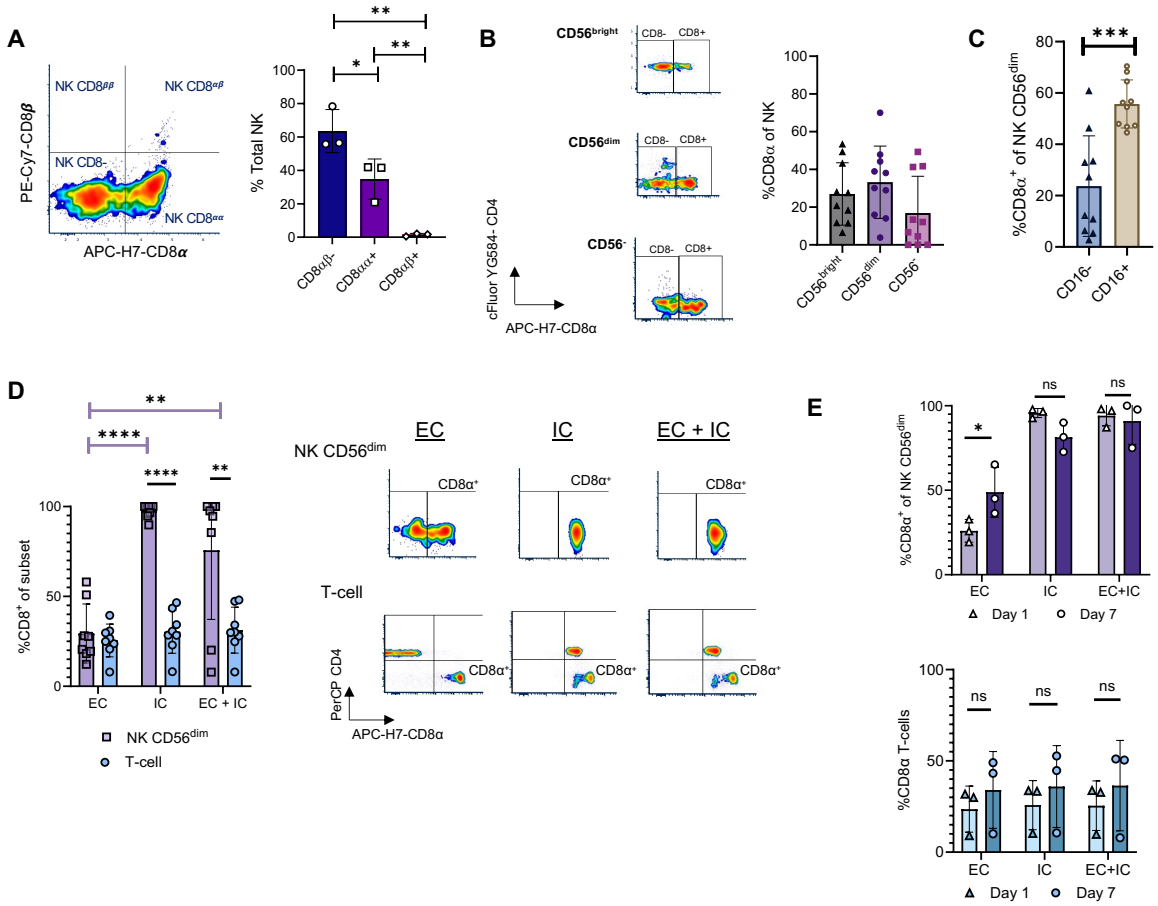

Fig. 5. CD8α$^+$ NK cells are prevalent in healthy US donors with ubiquitous intracellular CD8α expression. **(A)** Flow cytometry plot and percentage of CD8αα$^-$, CD8αα$^+$, CD8αβ$^+$, and CD8ββ$^+$ among total NK (N=3). **(B)** Percentage of CD8α$^+$ NK cells in different subsets based on CD56 expression (N=10). **(C)** Frequency of CD16 expression in CD8α$^+$ CD56^{dim} NK cells. **(D)** Frequency and representative flow cytometry plots of CD8α expression comparing CD56^{dim} NK cells and T cells with extracellular (EC), IC (Intracellular), and EC + IC CD8α staining. **(E)** Percent CD8α$^+$ in EC, IC, and EC + IC staining at day 1 and day 7 in CD56^{dim} NK cells and T cells. Statistical significance was measured using unpaired t tests, ns – no significance, *p<0.05, **p<0.005, ***p<0.001, ****p<0.0001.

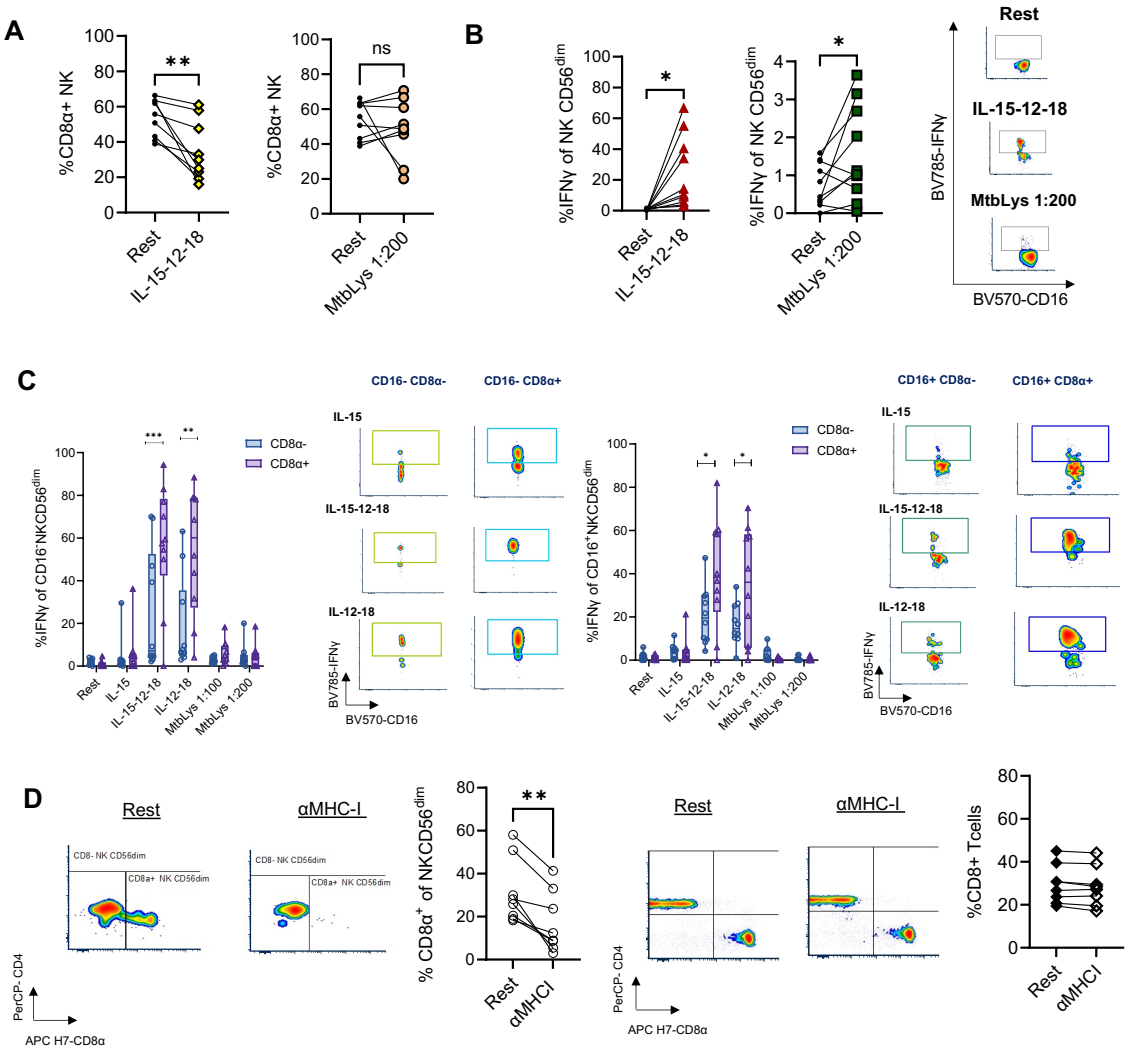

Fig. 6. CD8α$^+$ CD56^{dim} NK cells have enhanced response to cytokine stimulation. (**A**) Pairwise analysis of percent CD8α$^+$ NK cells upon stimulation with IL15/12/18 and MtbLys 1:200 (n=9). (**B**) Pairwise analysis and representative flow plots of intracellular IFNγ in NK CD56^{dim} upon stimulation with IL15/12/18 and MtbLys at dilution 1:200 (n=9). (**C**) Percent intracellular IFNγ$^+$ in CD8α$^+$ versus CD8α$^-$ CD56^{dim} NK cells comparing IL-15-Su, IL15-Su/12/18, IL-12/18, or MtbLys conditions (n=9). Both the CD16$^+$ (right) and CD16$^-$ (left) CD56^{dim} NK subpopulations are displayed. (**D**) Representative flow cytometry plots and paired analysis of percent change CD8α$^+$ with anti-MHC I for 15 hours among CD56^{dim} NK cells (left) and CD8$^+$ T cells (right) (n=8). Statistical significance was measured using paired t-test, with threshold of *p<0.05, **p<0.005, ***p<0.001. IFNγ: Interferon γ, Mtb Lys: *Mtb* whole cell lysate.

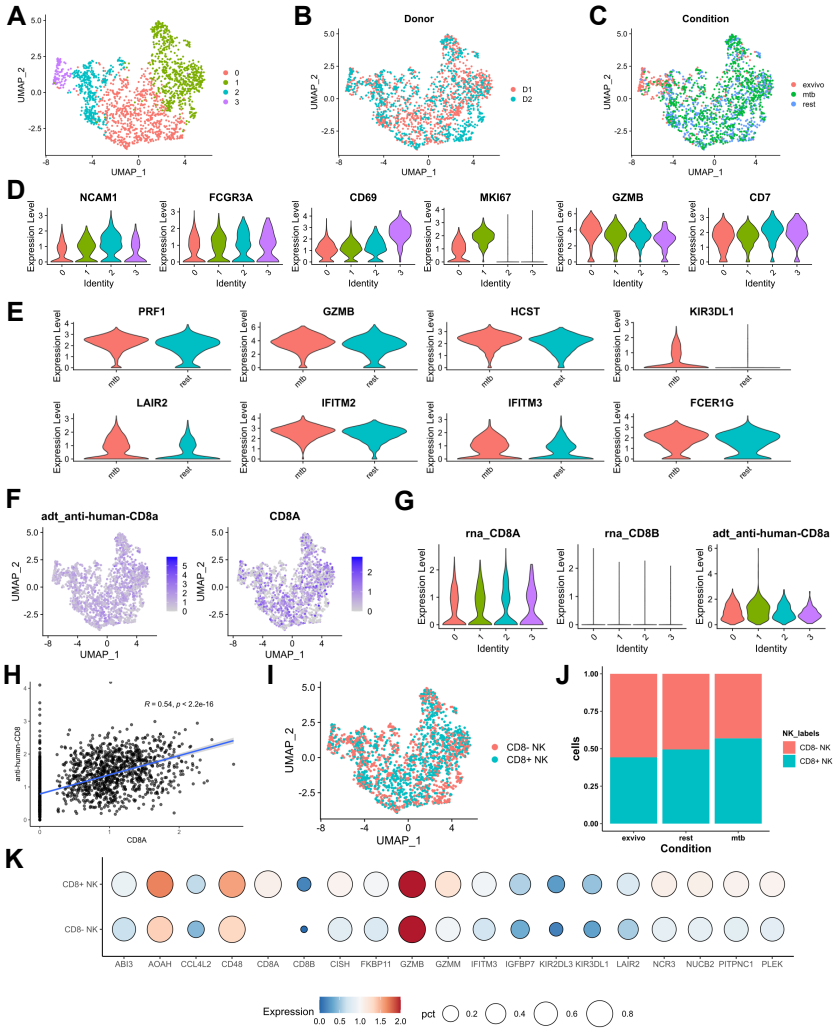

682 **Fig. 7. CITE-seq analysis of CD8α$^+$ vs CD8α$^-$ NK cells from two healthy donors reveals overlapping**
683 **transcriptomes. (A)** Results of clustering and uniform manifold approximation (UMAP) projection for all
684 NK cells. **(B)** UMAP reduction colored by Donor. **(C)** UMAP reduction colored by condition. **(D)** Violin
685 plots representing top six genes that were differentially expressed between the four NK cell clusters. **(E)**
686 Violin plots of the eight differentially expressed genes between resting and *Mtb* lysate condition. **(F)**
687 Distribution of NK cell expression of CD8 based on barcoded antibodies against CD8α and *CD8A*
688 transcript. **(G)** Violin plot of the expression of *CD8A* and *CD8B* transcripts, as well as CD8α surface
689 expression between the four NK cell clusters. **(H)** Correlation of CD8α expression between transcript and
690 protein measurement. **(I)** Annotated UMAP based on transcript expression of *CD8A* into CD8α$^+$ and
691 CD8α$^-$ NK cells. **(J)** Percent of NK cells expressing CD8A transcript between stimulation conditions. **(K)**
692 Dot-plot of genes differentially expressed between CD8α$^+$ and CD8α$^-$ NK cells.